Chapter 5

Excited-state perspectives of ultrathin films

In the previous chapter we have investigated the role of the finite thickness and the substrate for ground-state properties of thin oxide films and how they influence the film's electronic structure. However, new physical effects come into play for excited states that are not visible from the DFT ground-state perspective. These are contained in the self-energy Σ that connects the DFT-KS electronic structure to the quasiparticle spectrum observed in a photoelectron spectroscopy experiment as described in Sec. 2.3. Here we use the G_0W_0 approximation for Σ introduced in Sec. 2.3.2. We will show in this chapter that the G_0W_0 self-energy corrections for thin films differ from the bulk corrections mostly by polarisation effects that become important when a charged excited state is created in a dielectrically heterogeneous environment. Insulator films supported on a polarisable material, e.g. metal-supported oxide films, are prime representatives of this material class. We therefore expect that the substrate-induced image potential changes the photoelectron spectra and other charged-state properties beyond the ground-state effects discussed so far.

Unfortunately, reliable G_0W_0 calculations for metallic slab systems are not yet possible in the GW space-time method.[1] We have therefore chosen to study these effects for a prototypical insulator/semiconductor interface: NaCl on Ge(001). This system has been intensively studied with LEED [9, 29, 131, 132], SXRD [132], UPS [9], ELS-LEED [133], and STM [29]. In contrast to the metal-supported oxide films discussed in the previous Chapter, the thickness of the NaCl films on Ge(001) can be varied because the films assume

[1] Metallic systems require a different treatment of the time/frequency dependence in the space-time approach, which is currently under development [32].

the rocksalt structure of the bulk materials. We will demonstrate that also the G_0W_0 corrections are thickness-dependent. Most experiments, however, focussed on the surface properties of thick films (10–20 ML) [134–136] and no thickness-dependent measurements for thin films are available to date. For reference, the effects in free-standing NaCl slabs will be discussed, too. Before we present our results, we will briefly sketch out the type of G_0W_0 effects that are expected for thin films beyond the scissor shifts known from bulk systems [23, 56].

The dominant effect is introduced via the screened interaction W_0 and the long-range screening effects contained therein. We have already seen in Sec. 3 that the long-range screening and the image potential arising from dielectric discontinuities play a crucial role in practical G_0W_0 calculations for slab systems, where we have regarded them as artifacts of the periodic boundary conditions. Here we will use the same dielectric models to analyse the effect of the intrinsic dielectric steps at the surface of the thin film and its interface to the substrate. Using simplified models like this, Delerue *et al.* have previously investigated image potential effects for free-standing nanoparticles, wires, and films [137]. We will show that free-standing and supported films behave differently, although the physical basis of the effect is the same. Isolated films have two equivalent surfaces. The image potential induced by these surfaces will then shift all states of one type into the same direction: downwards for the valence states, upwards for the conduction states. Only the magnitude of the shifts might differ between the states, but we will see that this is not significant for NaCl. In a supported film, on the other hand, the image potential is asymmetric and will introduce a strong position-dependence of the self-energy that varies from one side of the film to the other.

Image effects are well-known in the context of core-level spectroscopy for atoms in the vicinity of dielectric interfaces e.g. in SiO_2/Si [138, 139]. They have also been discussed for the valence electron spectra of metal-supported oxide films of varying thickness [21, 140], but reliable theoretical calculations for a quantitative comparison are not available. The first G_0W_0 calculation that clearly demonstrated an image potential effect for an adsorbate was performed only very recently for a benzene molecule on graphite [31], where a drastic reduction of the molecular gap was found. As we will show in the following, the image effects can induce additional shifts of $\sim$0.5 eV for NaCl/Ge, thereby modifying the shape and the peak position of the electronic DOS.

The remainder of this chapter is organised as follows: first, we will discuss the free-standing NaCl films. Then we will turn to the supported NaCl films on a Ge(001) substrate. This system has not been theoretically investigated

before, in particular no atomistic structural model of the interface to Ge is available. We will therefore present our atomistic model that we developed from the experimental knowledge and DFT-LDA calculations, before we discuss the quasiparticle spectrum of ultra-thin films as well as its thickness dependence. Finally, we will use the experience gained in this section to reconsider screening effects in the electronic structure of the silica film on Mo(112), that had been discussed in Section 4.3.3 from the DFT-LDA perspective only.

5.1 Freestanding slabs

In this first part, we will investigate the G_0W_0 quasiparticle spectrum of free-standing NaCl films. Although such films cannot be prepared experimentally, they provide a simple system for illustrating the changes in the self-energy when going from a bulk material to a thin film. We thereby extend our study of the thickness dependence for free-standing films (Sec. 4.4) to excited-state effects. We use NaCl here instead of the oxides in order to compare to the supported NaCl films presented in the next Section. We will show in the following that the band gap of free-standing ultra-thin NaCl films is larger than the corresponding bulk band gap. The increase of the band gap due to a surface contribution to the self-energy has been predicted from model calculations [137]. Mainly long-range screening effects are responsible for this, and we will show that a dielectric model can semi-quantitatively reproduce the results from our *ab initio* G_0W_0 calculations. However, we find that the model calculations overestimate the effect systematically.

For our calculations, we consider free-standing NaCl slabs with a (1×1) (001) surface containing two to five NaCl layers, using the theoretical bulk lattice constant to define the surface unit cell. As shown in Sec. 3.3.3, we correct for the finite vacuum effect in G_0W_0 calculations. We then find that a vacuum thickness of 10 Å is sufficient to decouple the films. The films are fully relaxed in DFT-LDA, but the relaxations are small, as is well known for the (001) surface of sodium chloride [141]. The Na ions relax inward by 0.046 Å (1.7% of the inter-layer spacing) and the Cl ions outward by 0.040 Å (1.4%) for films with 5 or more layers. Thinner films show slightly deviating absolute values, but the same sign (e.g. 2 layers: Na -2.7%, Cl +2.2%). The values for the Cl relaxation agree well with experiment, but those for the sodium relaxation are smaller than the experimental results from LEED (Na -2.9%, Cl +1.4% [141]). However, the surface relaxation does not play any role for the G_0W_0 corrections. The quasiparticle energies presented in the following include all corrections and extrapolations discussed in Sections

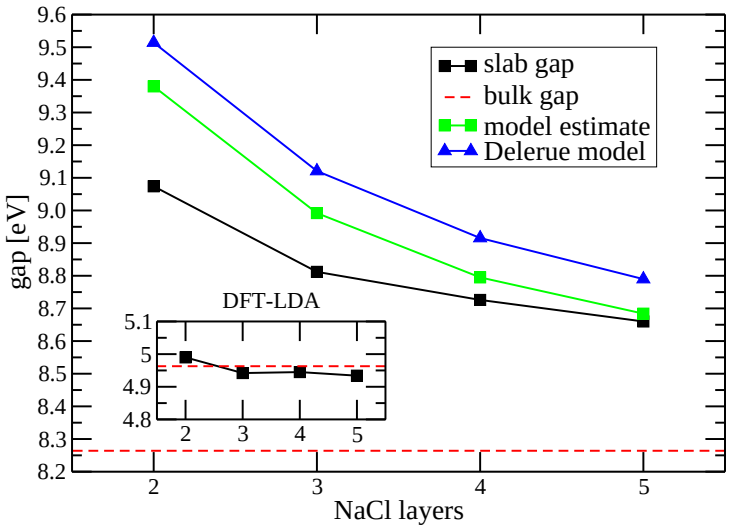

Figure 5.1: Quasiparticle gap of free-standing NaCl slabs of varying thickness. The slab data is corrected for the bcut error (cf. Section F.3.3). The model estimate refers to the image potential at the centre of the slab, see text.

3.3.2, 3.3.3, and F.3.3.

The electronic DOS at the LDA level is indistinguishable from bulk NaCl at all thicknesses, and we therefore refrain from showing it here. The observation hat the electronic structure is not affected by the thickness is easily explained. As mentioned above, the atomic structure deviates only very little from the ideal bulk positions and does therefore not introduce significant changes in the electronic structure. Furthermore, the localised character of the valence states makes them insensitive to the slab thickness. The delocalised, dispersive conduction band on the other hand hybridises with a surface resonance (cf. Fig. 5.5), pinning the gap at about 4.94 eV close to the bulk gap at 4.96 eV. When G_0W_0 corrections are applied, this invariance of the gap to the thickness is removed (cf. Fig. 5.1). At a thickness of two layers, the quasiparticle gap is 0.8 eV larger than in the bulk. With increasing thickness, it slowly reduces towards the value of the bulk band gap. The other states behave similar to the band edges states, i.e. the main effect of the G_0W_0 correction is a scissor shift of the bands. This is well known from bulk G_0W_0 calculations [23, 62]. Other significant changes besides this thickness-dependent scissor shift are not observed.

We will now show that the change of the dielectric constant at the surface and the resulting image potential is responsible for the thickness dependence of the quasiparticle gap. For this purpose, we compute the image potential for a homogeneous model dielectric slab (thickness s, dielectric constant ε).

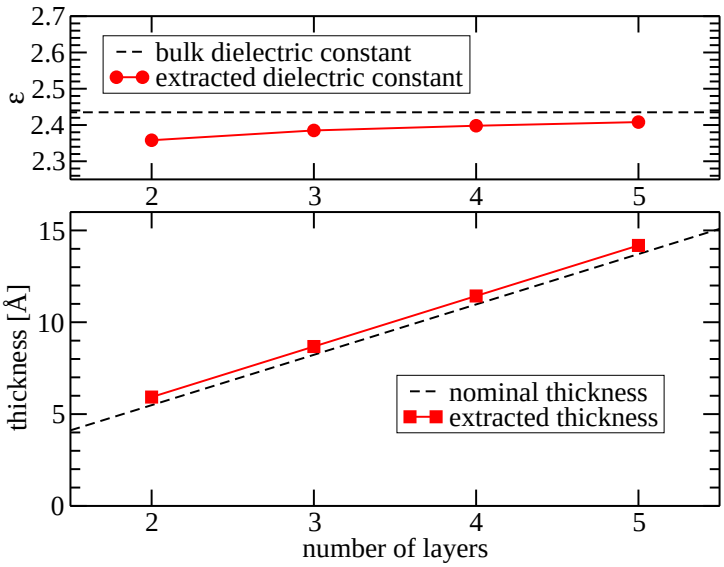

Figure 5.2: Model parameters extracted from the dielectric tensor of the repeated-slab systems.

This model is the basis of Delerue's "surface contribution to the self-energy" [137], given by

$$\Delta = \frac{2}{\varepsilon s}\left(0.21883\frac{\varepsilon - 1}{\varepsilon + 1} + \ln\frac{2}{\varepsilon + 1}\right) , \tag{5.1}$$

which corresponds to the expectation value of the image potential for a sine model function. Alternatively, we employ the value of the image potential in the slab centre to estimate the magnitude of the image potential effect. The necessary parameters, i.e. the slab thickness s and its dielectric constant ε, are extracted from the dielectric tensor of the repeated slab system as described in Section 3.3.3. The extracted parameters are shown in Fig. 5.2. The dielectric constant depends only weakly on the slab thickness and is close to its bulk value. Also the effective thickness is in very good agreement with the nominal thicknesses of 2.74 Å per NaCl layer. We thus find that the computed model parameters are very close to intuitive estimates, indicating that the dielectric properties of the slabs are bulk-like.

In Fig. 5.3 we show the image potential computed from the parameters for 2–5 NaCl layers. The image potential is positive inside the slab and becomes smaller when the thickness is increased. At the surfaces, the image potential diverges, which is an artifact of the dielectric discontinuities in the step profile chosen as model here. A smoothly varying dielectric constant yields a smoothly varying image potential. Since the image charge method that we have developed (cf. Sec. B.1) allows us to use arbitrary profiles

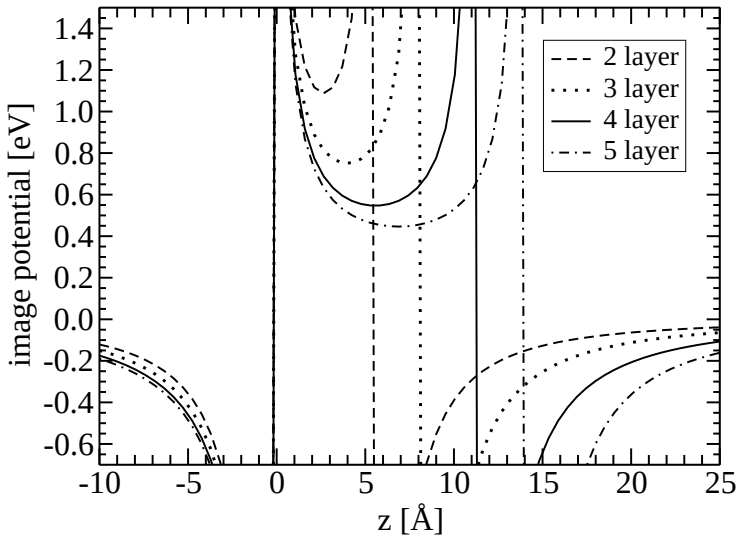

Figure 5.3: Image potential in the dielectric slab models for freestanding NaCl slabs of varying thickness.

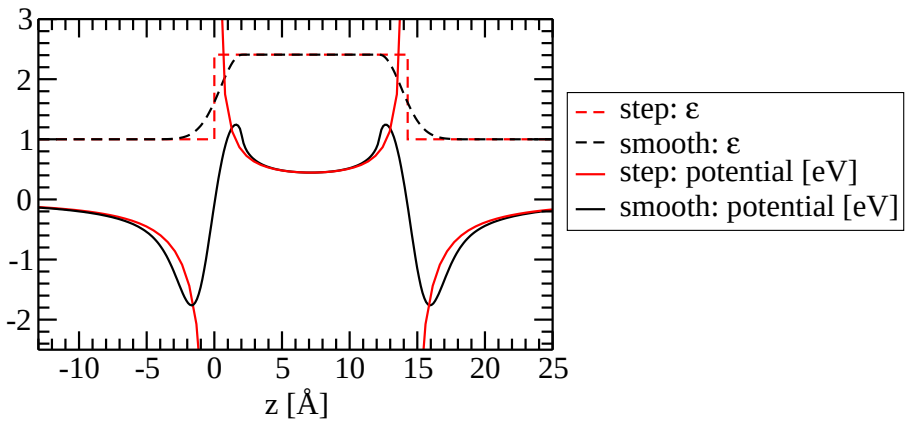

Figure 5.4: Comparison of computed image potentials for a discontinuous step profile and a smooth, Gaussian-derived profile (see text). The parameters correspond to a 5-layer NaCl slab.

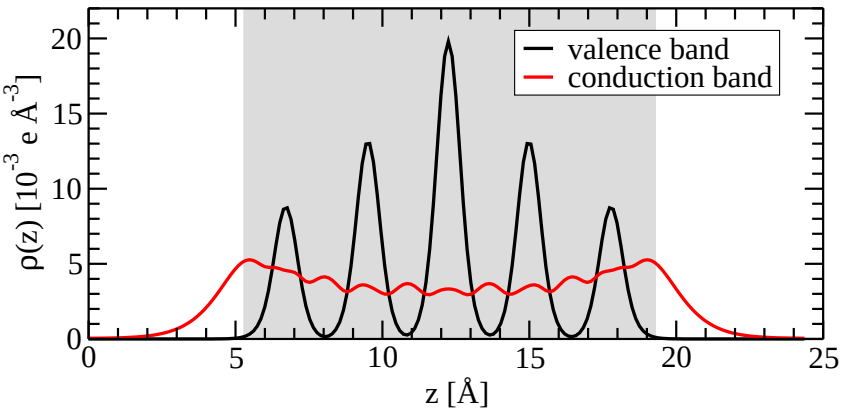

Figure 5.5: Partial density of the valence band maximum and conduction band minimum for a 5 NaCl layers. The grey region indicates the size of the dielectric model, showing that the conduction states are not confined within it.

$\varepsilon(z)$, we can investigate the influence of the transition between the slab and the vacuum. This is demonstrated in Fig. 5.4, where we compare the image potential of the step profile with that of a smooth profile obtained by introducing a Gaussian-shaped transition region

$$\varepsilon(z) = \begin{cases} 1 + (\varepsilon - 1)e^{-\pi/4(z/t-1)^2} & z < t \\ \varepsilon & t \leq z \leq s - t \\ 1 + (\varepsilon - 1)e^{-\pi/4((z-s)/t+1)^2} & z > s - t \end{cases} . \tag{5.2}$$

The broadening of the Gaussian is controlled by the transition width t (here: t=2 Å) and the prefactor ensures that the average dielectric constant agrees with the step model. We emphasise that this profile serves only as an example for a smooth profile and is not necessarily more realistic than the step profile. We also note that the concept of a local dielectric constant is not well defined. We therefore restrict ourselves to simple models consistent with the dielectric tensor. In Fig. 5.4, we compare the two resulting image potentials for a 5-layer slab. The Gaussian profile yields a continuous image potential in the transition region. The divergences of the step profile is replaced by minima and maxima. In the vicinity of these, the potential is slightly enhanced over that of the step profile. Away from the transition region, the image potentials for the two profiles agree with each other very well. We will therefore restrict our further discussions to the simpler step profiles and avoid to include the image potential in the transition region as far as possible.

Focussing on the average shift ΔW of the potential inside the slab, we can use the finding of Sec. B.2 to estimate the change in the quasiparticle gap:

ΔW acts as an additional scissors shift. To estimate ΔW semi-quantitatively and to avoid the divergence at the surface, we take the value at the slab centre and assume that the variations at the surface cancel out to a large degree. This is justified by the observation that at least the conduction states are not fully confined inside the model slab thickness (cf. Fig. 5.5), but extend out into the vacuum where the model image potential is negative. This approach differs from the Delerue model [137], where a sine model function confined to the slab is used to compute the expectation value of the image potential inside the slab. The Delerue model therefore predicts *larger* effects than our slab-centre method. The resulting estimates for the band gap of the NaCl slabs have been included in Fig. 5.1. Taking into account the rather crude approximations involved, they show a reasonable agreement (within about 30% for the slab-centre method or 50% for the Delerue model) with the observed increase in the quasiparticle gap.

We conclude that the change in the dielectric constant when going from NaCl to the vacuum induces an image potential inside the NaCl slabs for charged excitations. The quasiparticle gap of the slab reflects the modified screening and increases compared to the bulk value. These image-potential effects are part of the G_0W_0 self-energy, but since they are due to the long-range correlation, they are absent from the DFT-LDA exchange-correlation potential. Moreover, a simple dielectric model is sufficient to reproduce the results of the full *ab initio* G_0W_0 calculation to within 30%. It can thus be used to estimate the magnitude of image-potential effects in the quasiparticle energies, but it cannot replace the full calculation if a quantitative answer is required.

5.2 NaCl films on Ge(001)

In this section the quasiparticle spectrum will be discussed for the realistic case of NaCl films supported on Ge, which can be prepared and investigated experimentally. We therefore briefly summarise what is experimentally known about this system (Sec. 5.2.1). Then we present the atomistic model derived from the experimental results using DFT-LDA calculations (Sec. 5.2.2). The G_0W_0 calculations will be discussed in Sec. 5.2.3.

5.2.1 Experimental situation

Supported sodium chloride films are prototypical systems for studying the properties of thin insulator films [9, 10, 29, 131, 142]. NaCl films are mostly grown on metallic substrates, e.g. Al [142] or Cu [10], but for the G_0W_0

calculations we will focus on a semiconducting substrate: Ge(001). Well-ordered, crystalline NaCl films with a thickness of a few monolayers (ML) can be grown on Ge(001) with high quality [9], since the lattice mismatch between Ge (5.66 Å) and NaCl (5.63 Å) is only 0.5%. Correspondingly, the [100] and [010] directions of the substrate and the film are aligned. Films of varying thicknesses up to several nanometer can be grown by sublimation of NaCl onto a clean Ge(001) surface kept at 100 K, followed by annealing at 400 K for a few minutes. From Auger electron attenuation [9] and later STM measurements [29] it was concluded that initially a double-layer film forms on which further single layers grow layer by layer. While STM pictures for a 2ML film exhibit a NaCl 1×1 pattern at the surface [29], LEED and SXRD experiments show a p(2×1) unit cell corresponding to the typical buckled-dimer reconstruction of the Ge(001) surface [9, 29, 132]. It has therefore been concluded that the Ge dimers remain intact under the film, supported by ELS-LEED which detects the Ge surface states even when a 20 ML NaCl film is grown on top [133].

The interaction of the sodium chloride film with the Ge(001) substrate is rather weak. This leads to the "carpet" growth mode over mono-atomic steps of the substrate, where the NaCl film smoothly covers the substrate [29, 131]. From the extent of the transition region, Schwennicke *et al.* have estimated a binding energy of 0.13 eV per Ge atom [131]. The atomic structure of the interface between Ge and NaCl is not known from experiment. To explain their results from surface X-ray diffraction, Lucas *et al.* suggested that an additional sodium atom is present in the surface unit cell [132], but a detailed structural analysis was not performed. On the other hand, Ernst *et al.* have found that preadsorbed sodium atoms break the Ge dimers and modulate the structure of an adsorbed NaCl film up to about 10 ML thickness [143]. We therefore consider the presence of additional sodium atoms in the unit cell unlikely for films deposited on the clean Ge(001) surface as they do not show this modulation.

For films of two to three ML thickness, STM experiments can be performed with atomic resolution in a small energy window of 1.5 eV to 2.7 eV tip bias [29]. This energy range lies inside the gap of the NaCl overlayer, i.e. no states with dominant NaCl character contribute to the tunnelling. Nevertheless, the STM pictures must reflect the structure of the surface of the NaCl film as they show a 1×1 square pattern with a height corrugation of 0.5 Å. Furthermore, only one type of ion is imaged. Glöckler *et al.* have concluded that the tunnelling is from Ge bulk and interface states that are "modulated" by the NaCl overlayer. They have speculated that variations in the local work function could be responsible for the modulation and that Na^+ ions are imaged as the bright spots. The STM experiments have also

confirmed the carpet overgrowth of mono-atomic steps and the film thickness deduced from Auger electron spectroscopy. The apparent thickness of a single NaCl layer as measured in STM is 2.0±0.3Å, somewhat smaller than the geometrical thickness of 2.8Å, but such a difference is not unusual for insulator films [144].

From the experimental investigations, the following questions remain open:

1. The atomic structure of the interface between Ge and NaCl,
2. the observed preference for the p(2 × 1) surface unit cell,
3. the preference for an initial double layer, and
4. the source of the STM contrast.

We will address these questions in the following using DFT-LDA *ab initio* simulations. The surfaces are simulated in the repeated slab approach. The Ge substrate is modelled by 6 layers, saturated with hydrogen at the bottom. The bottom two layers were kept fixed during the relaxations. We verified the reliability of this approach by comparing to a 12 layer Ge slab, which yields essentially identical structural parameters and adhesion energies. A p(2 × 1) surface unit cell with the experimental lattice constant (5.66 Å) was used. The separation of neighbouring slabs was ∼9 Å between the outermost atoms which proved to be sufficient to avoid interactions across the vacuum. The use of asymmetric slabs in the repeated-slab approach introduces an artificial electric field across the slab when the work function of the two surfaces differ. A dipole correction was used to correct for this [78].

5.2.2 Atomic structure of the interface

The identification of the most stable interface is described in Sec. D.3. The resulting atomic structure for a 2ML NaCl film is shown in Fig. 5.6. We find that a negatively charged chloride ion is situated above the lower ("down") atom of the Ge dimer, while a sodium ion bridges two "up" dimer atoms. This suggests that electrostatic interactions may be responsible for the observed geometry, since the *down* (*up*) atom is expected to carry a positive (negative) partial charge. We have therefore computed the electrostatic potential of the clean Ge surface at the geometry of the adsorbed NaCl layer (cf. Fig. 5.7). The shape of the electrostatic potential agrees qualitatively very well with the adhesion energy line scans presented in Fig. D.5. It shows a strong corrugation along the dimers, and a much flatter one in the perpendicular direction (Fig. 5.7 a). The electrostatic potential also helps to understand the atomic

relaxation in the bottom layer of the NaCl film (Fig. 5.7 b). The chloride ion above the *down* Ge atom relaxes towards this atom, in agreement with the very steep electrostatic potential in this region. Likewise, the sideward relaxation of the second chloride ion in the bottom NaCl layer is driven by the electrostatic repulsion of the occupied dangling bond state. The preference for the Cl-*down*/Na-*up* combination explains why only a p(2×1) pattern is observed in LEED and SXRD. Other dimer patterns such as c(4×2) would inevitably include the opposite combinations, which would be strongly disfavoured due to the electrostatic repulsion. Interestingly, also the adhesion of NaCl films on Cu(311) surfaces is effectuated by electrostatic interactions between the ions in the film and charge modulations at the substrate surface, which are in this case caused by the Smoluchowski smoothening at the corrugated Cu(311) surface [10]. This implies a surprising similarity between the NaCl/metal and NaCl/semiconductor interface in this case, which is further supported by the carpet overgrowth of mono-atomic steps for both cases.

The adsorption of the NaCl layers influences the Ge dimer, too. While the dimer is tilted by 19° at the clean Ge surface, this angle reduces to 10° when NaCl is adsorbed with Cl on top of the *down* atom[2]. The *down* atom relaxes upwards by 0.24 Å and the *up* atom relaxes downwards by 0.12 Å. The dimer bond length increases slightly by 1%. The redistribution of the electrons upon the adsorption of the NaCl overlayer was investigated by the density difference

$$\Delta\rho = \rho(\mathrm{Ge} + \mathrm{NaCl}) - \rho(\mathrm{Ge}) - \rho(\mathrm{NaCl}) \ , \tag{5.3}$$

shown in Fig. 5.8 across the dimer. The density is increased between the chloride ion and the *down* Ge atom as well as between the sodium ions and the *up* Ge atoms. The ionicity (charge separation) in the Ge dimer appears to be slightly increased, too. The bonding characteristics is probably best described as a weak Lewis acid/base complex, an intermediate form between an ionic and a covalent bond [94].

We have also simulated the STM experiments in the Tersoff-Hamann approximation, reported in Sec. D.4. In summary, we find strong evidence that the tunnelling is – as suggested – from the Ge states. These hybridise with the chlorine $3p$ orbitals of the film, and the bright spots in the STM pictures must then be assigned to the Cl ions and not – as suggested in [29] to Na. We determined the average apparent heights of the NaCl layers from our simulation and find good agreement with experiment. We are however not able to reproduce the experimental corrugation laterally resolved STM pictures. We find a (2×1) pattern with an apparent height difference of 0.3 Å

[2]When Na is adsorbed on top of the *up* atom, the dimer angle becomes 15°.

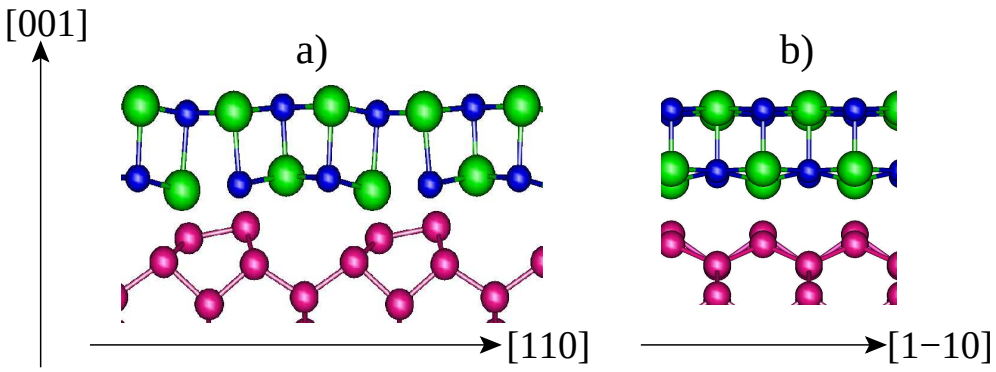

Figure 5.6: Side views of the optimised geometry for the 2 ML NaCl film on Ge(001) a) along the dimers and b) perpendicular to them. The colour coding is as follows: Ge (magenta), Na (blue), and Cl (green).

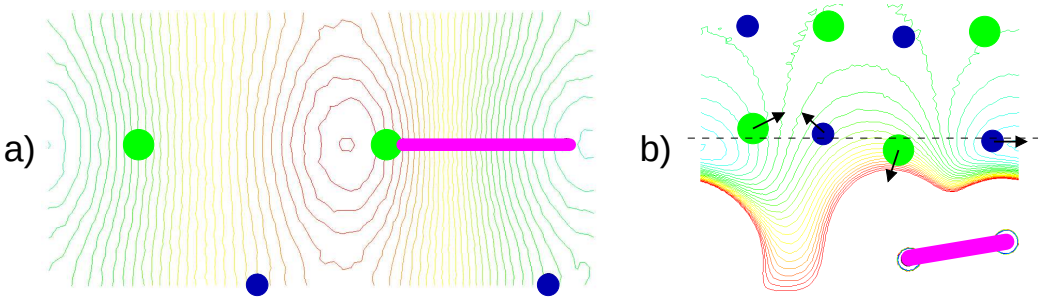

Figure 5.7: Electrostatic potential maps for the clean Ge surface (in the Ge/NaCl geometry). a) Top view at the average height (see dashed line in b) of the bottom NaCl layer (spacing 0.02 V). b) Side view through the dimer (spacing 0.05 V). The potential increases from blue-green to red. The circles indicate the atomic positions of the NaCl overlayer, the bar the Ge dimer (colours as in Fig. 5.6). The arrows indicate the direction of the electrostatic forces that drive the relaxation in the bottom layer.

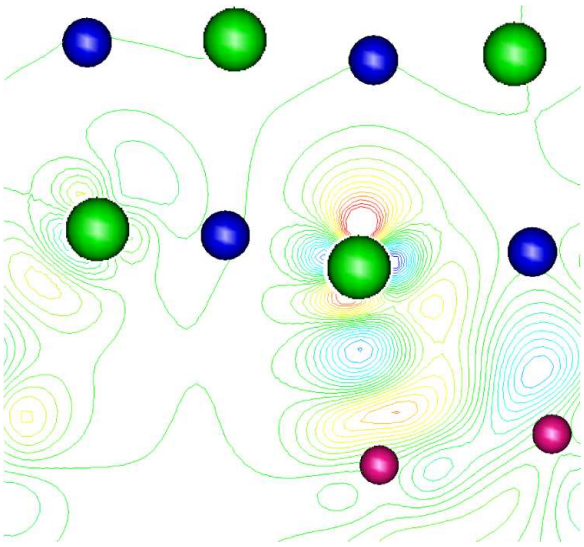

Figure 5.8: Electron density difference map across the Ge dimer. Red indicates a reduction in density, blue an increase. The spheres indicate the atom positions (colours as in Fig. 5.6).

between the bright features. Glöckler *et al.* report a 1×1 pattern in the STM. The discrepancy might be due to limitations in the theoretical modelling of the STM (cf. Sec. D.4) or to the limited resolution in the experiment from 1996 [29]. New STM experiments might help to clarify this issue.

For thicker films we used the interface model from the 2ML film as the starting geometry for the relaxation. In general, we find that the buckling in the NaCl film visible in Fig. 5.6 a) is reduced when further layers are added. As a measure for the relative stability of the films, we show the formation energy per NaCl formula unit from bulk NaCl with the Ge lattice constant (other lattice constants would only lead to a constant offset) in Fig. 5.9. The stability of the film increases monotoneously with increasing thickness. This suggests that the thermodynamically favoured structures are three-dimensional islands rather than flat films. The experimentally observed preference for flat films must therefore be attributed to kinetic limitations. This appears plausible since the thin films are annealed at only 400 K [9], well below the melting point of NaCl (1074 K, [94]). The observation that the substrate must be kept at very low temperatures during the deposition [9] supports this conclusion, too.

In summary, we have developed an atomistic model of the NaCl/Ge interface. The Ge dimers remain intact and buckled under the film as suggested from ELS-LEED. The chloride ions are found to adsorb on top of the *down*

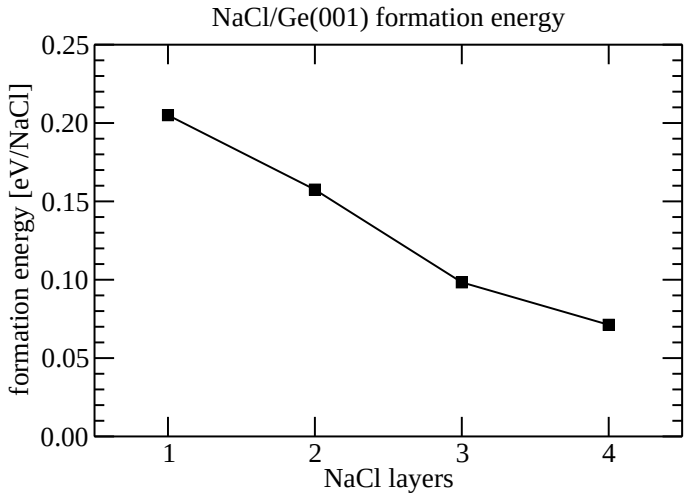

Figure 5.9: Formation energy per NaCl unit of the adsorbed NaCl film on Ge(001) as a function of the film thickness.

atom of the Ge dimer. This film geometry is stabilised by the electrostatic attraction between the ions in the film and the partially charged dimer atoms. When the overlayer is shifted perpendicular to the dimer axis, the adhesion energy changes only very little. Since the energy differences involved may be below the accuracy of the present DFT-LDA calculations the position of the film along $[1\bar{1}0]$ cannot be determined without doubt, but also in experiment this position might not be fixed. We will focus in the following only on the most stable interface found in the DFT-LDA calculations, where one Cl atom is located on top of the *down* atom of the buckled Ge dimer.

5.2.3 G_0W_0 calculations

We now turn to the results of the G_0W_0 calculations, the main topic of this chapter. Since experimental spectroscopy data for ultrathin films is not available, we will mainly focus on the physical effects and trends visible in our G_0W_0 calculations. We will briefly address the comparison to the relevant UPS studies for thick films later. We note that the G_0W_0 calculations are numerically converged to only 0.1 eV to 0.2 eV in the quasiparticle energies. To improve the accuracy, corrections must be included to account for

- the under-convergence in the band cutoff (Sec. F.3.3),
- the finite **k**-point sampling (Sec. 3.3.2), and
- the finite-vacuum effect (Sec. 3.3.3).

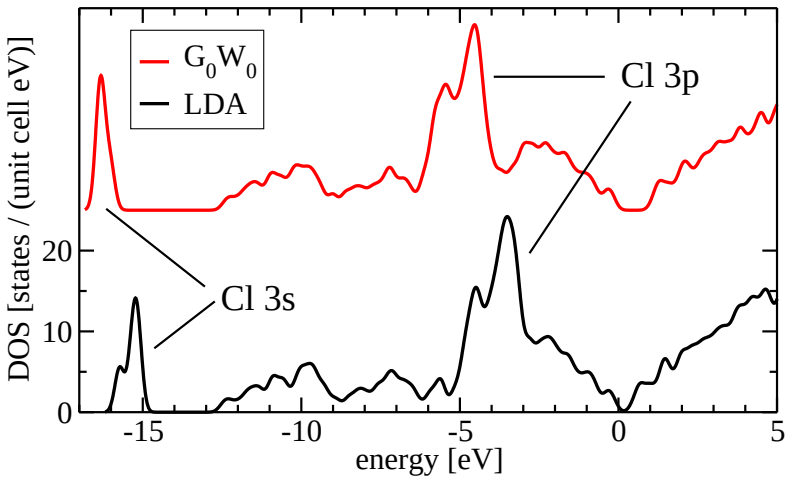

Figure 5.10: DOS for the supported 2ML NaCl film on Ge(001) at the DFT-LDA level and the G_0W_0 level. The slab valence band maximum defines the energy zero.

However, all three corrections mainly affect the absolute band position, and have almost the same value for all NaCl thicknesses considered. For simplicity, we will not include these corrections when we discuss the effects within the NaCl valence bands. We estimate that the relevant differences in the G_0W_0 corrections within the Cl $3p$ and $3s$ bands are obtained with an accuracy of 0.05 eV–0.1 eV.

We have also computed the G_0W_0 quasiparticle band structure for the Ge bulk and the clean Ge surface. The quasiparticle gap corrections computed for bulk Ge (∼0.7 eV, **k**-dependent) agree reasonably with previous calculations [23]. For the surface, we obtain a good agreement with the results of Rohlfing [61] within the valence band. The correction to the quasiparticle gap is larger by ∼0.2 eV when we include the finite-vacuum correction. We attribute this discrepancy to the more accurate treatment of long-range screening in our calculations (cf. Sec. 3).

In Fig. 5.10 we present the total DOS for two NaCl layers on a 6 layer Ge substrate. The DOS is shown for the DFT-LDA and for DFT-LDA with G_0W_0 corrections, denoted as G_0W_0 DOS in the following. Two features can be attributed to the NaCl-derived states: the Cl $3s$ peak around -16 eV and the Cl $3p$ states at around -5 eV. The most important change when comparing the LDA and G_0W_0 DOS is the shift of the NaCl bands relative to the Ge states. Such a shift is not surprising since the G_0W_0 corrections in bulk NaCl are much larger (3.3 eV) than for the Ge bulk (0.7 eV). However, also the shape of the NaCl-derived features changes when going

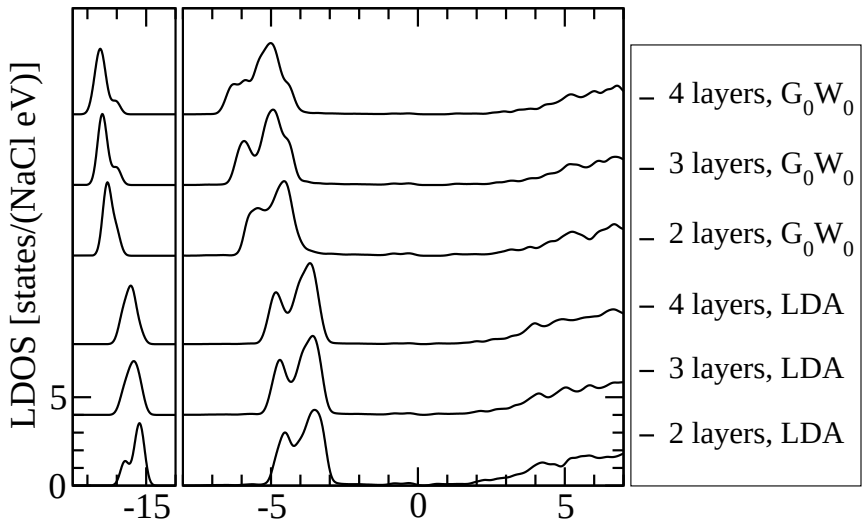

Figure 5.11: LDOS projected on the NaCl film region for supported NaCl films on Ge(001) at the DFT-LDA level and the G_0W_0 level. The slab valence band maximum defines the energy zero.

from DFT-LDA to the G_0W_0 DOS, indicating that the G_0W_0 shifts for NaCl are not uniform. As we will show below, they are caused by the position-dependence of the self-energy that results from the dielectric response of the substrate. To compare NaCl films of varying thickness, we will use the region-projected LDOS described in Sec. C.2. The normalised DOS for 2–4 ML films is shown in Fig. 5.11. While the DOS in the Cl-3p region is essentially thickness-independent at the level of DFT-LDA, the G_0W_0 corrections introduce a visible thickness dependence in the shape and the width of the NaCl bands. This reemphasises our earlier observation that the bulk corrections are not transferable to thin films. Rather, excited states undergo additional thickness-dependent and substrate-specific changes that are neither visible from a ground-state perspective nor predictable from bulk G_0W_0 calculations for the separate fragments only.

Our first step to approach the unusual G_0W_0 shifts of the supported films will be to prove that the self-energy corrections are position-dependent. However, most of the bands are more or less delocalised over the film, which makes it difficult to directly determine the local self-energy contributions. To extract position-dependent shifts, we employ the atomic orbital projection technique described in Sec. D.1 to determine the localisation of the state. Several states are dominated by the orbitals of only one atom. When the G_0W_0 corrections of the bands are plotted against this projection, we obtain a linear dependence once the contribution from a single atom exceeds

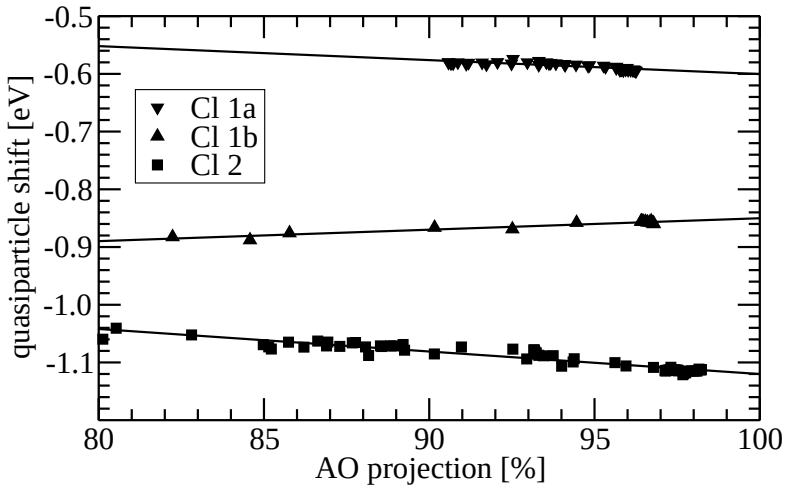

Figure 5.12: Extraction of orbital-dependent G_0W_0 shifts for the example of Cl 3s orbitals of 2ML NaCl/Ge. For the atom labelling, see Fig. 5.13 a).

	Cl 3s					Cl 3p				
ML	1a	1b	2	3	4	1a	1b	2	3	4
2	-0.60	-0.85	-1.12			-0.79	-1.10	-1.40		
3	-0.54	-0.84	-1.01	-1.06		-0.70	-1.08	-1.29	-1.47	
4	-0.53	-0.83	-0.99	-1.06	-1.16	-0.76	-1.04	-1.28	-1.33	-1.52

Table 5.1: Extrapolated G_0W_0 shifts (relative to the Ge vbm) for chlorine orbitals in supported NaCl films (see text). The position of the Cl atoms is given in layers, where 1 is closest to the Ge. The first layer contains Cl ions in different position, on top of the Ge dimer (1a) and between two Ge dimers (1b), cf. Fig. 5.13 a).

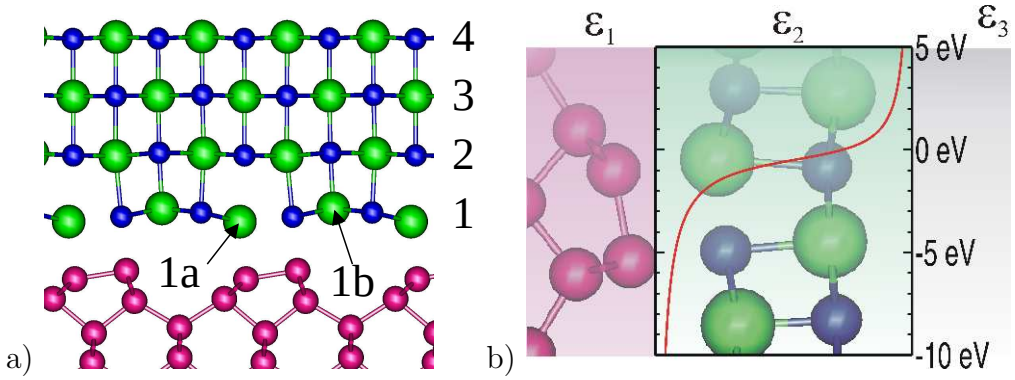

Figure 5.13: a) Cl positions in the supported 4 layer NaCl film for the position dependence of the G_0W_0 shifts. b) The dielectric model for a 2ML slab (rotated by 90°): the Ge (ε_1), NaCl (ε_2), and vacuum (ε_3) regions are shaded. The red line shows the image potential.

∼80% (cf. Fig. 5.12). These orbital-dependent G_0W_0 corrections are linearly extrapolated to 100%; the results are listed in Tab. 5.1. The extrapolated shifts in the first layer differ considerably between the two nonequivalent positions 1a (Cl on the dimer) and 1b (Cl between the dimers, cf. Fig. 5.13 a), while the atoms in higher layers behave very similarly. We do therefore not differentiate between them.

The most important trend is that the quasiparticle energies are shifted upward in the vicinity of the Ge substrate – a direct result of the image potential that forms at the interface of the NaCl film ($\varepsilon \approx 2.4$) and the Ge substrate ($\varepsilon \approx 14$), cf. Fig. 5.13 b). A similar effect, but opposite in sign results from the dielectric step at the surface (vacuum $\varepsilon = 1$). We again use a dielectric slab model to compute the image potential within the NaCl film. For this, the Ge substrate and the NaCl films are represented by homogeneous slabs with dielectric constants as stated above. The thickness of the NaCl film was assumed to be 2.8 Å per layer. In Fig. 5.14, we compare the extrapolated shifts from Tab. 5.1 to the image-potential effect computed from the dielectric slab model for the films of 2–4 layers thickness by plotting the following model self-energy for the occupied NaCl states

$$\Sigma(z) = \Delta\Sigma - \frac{1}{2}V(z) \tag{5.4}$$

where we include the correct prefactor for the image potential (cf. Sec. B.2). $\Delta\Sigma$ accounts for the different corrections to the Ge and NaCl states. To a first approximation, $\Delta\Sigma$ for the Cl $3p$ states is estimated from the bulk

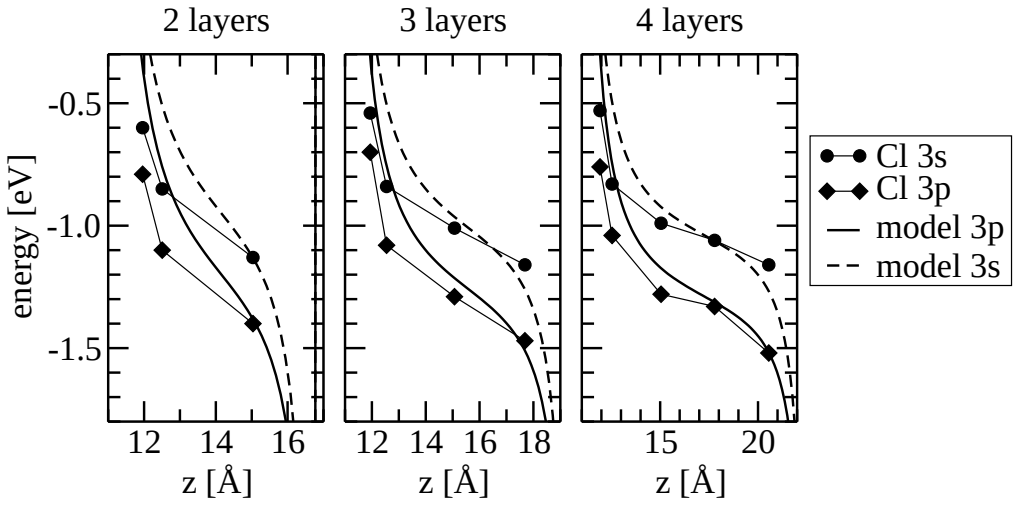

Figure 5.14: Comparison of the extrapolated G_0W_0 orbital shifts to the image potential of the dielectric slab model (cf. text).

corrections of the quasiparticle gap Δ^{gap}

$$\Delta\Sigma = \frac{1}{2}\Delta^{\mathrm{gap}}(\mathrm{Ge}) - \frac{1}{2}\Delta^{\mathrm{gap}}(\mathrm{NaCl}) = -1.3\,\mathrm{eV}\ . \tag{5.5}$$

For the $3s$ states, we assume $\Delta\Sigma = -1.05\,\mathrm{eV}$ to account for the different shifts of $3s$ and $3p$ states. We find a reasonable, qualitative agreement, highlighting that mainly the dielectric response effects are responsible for the position dependence of the G_0W_0 self-energy.

We now turn to the question of how delocalised states are affected by this self-energy. We emphasise again that the position-dependence was extracted from the G_0W_0 shift of only partially localised states by extrapolating to the "pure" orbitals. We now go the opposite way. The G_0W_0 correction to the LDA energies is obtained in the perturbative approach as

$$\Delta\epsilon_{n\mathbf{k}} = \langle\psi^{\mathrm{LDA}}_{n\mathbf{k}}|\Sigma - V_{\mathrm{xc}}|\psi^{\mathrm{LDA}}_{n\mathbf{k}}\rangle\ , \tag{5.6}$$

i.e. we freeze the composition of the quasiparticle state at the level of the LDA. Consequently, the G_0W_0 corrections will reflect the position-dependence of the self-energy according to the local weight of the state in the various layers. Most of the states in the Cl $3p$ valence region are delocalised over the NaCl film and the G_0W_0 shifts lie between -0.7 and -1.4 eV, the shifts for the bottom and top layer, respectively. Applying the G_0W_0 corrections then leads – in addition to the shift with respect to the Ge vbm – to a broadening of the DOS in the Cl $3p$ region because the corrections vary between the

orbital	2	3	4
4σ	–2.99	–3.09	–3.14
π_1	–2.31	–2.36	–2.41
π_2	–2.18	–2.24	–2.33
5σ	–1.81	–1.90	–1.96
π_1^*	+3.05	+3.20	+3.29
π_2^*	+3.52	+3.58	+3.73

Table 5.2: Quasiparticle shifts (with respect to Ge vbm) for p-derived orbitals of CO adsorbed on Ge-supported NaCl films with 2–4 layers.

different states (cf. Fig. 5.11). The situation for the Cl 3s states is different: we observe a sharpening of the peak. At the DFT-LDA level, it consists of distinct, but close-lying states associated with the different Cl position. The shift in the peak positions is caused by a gradual increase in the electrostatic potential throughout the film and causes the apparent broadening. This is counteracted by the image potential contained in the G_0W_0 self-energy which has the opposite sign. After applying the G_0W_0 corrections, the peak positions are closer and we find a sharp peak with a small shoulder $\sim 0.5\,\mathrm{eV}$ higher in energy, which can be attributed to the Cl atom in the bottom layer of the film situated above the dimer. This shift is dominated by the image potential, whereas the electrostatic potential alone would lead to a downward shift (visible for example in the LDA DOS for 2ML in Fig. 5.11). We observe a similar shoulder at the top of the Cl 3p orbitals. The broadening-induced increase in the band width and the additional shoulders should be detectable by photoelectron spectroscopy for ultrathin NaCl films on Ge, but such measurements are unfortunately not available, yet.

The quasiparticle spectrum contains the contribution of the energy dispersion (which, for NaCl, is accurately described within DFT-LDA) and of the image potential. The influence of the latter can be identified best for localised states with a small energy dispersion. The conduction band of the NaCl films consists of highly dispersive, delocalised states that additionally hybridise with the Ge conduction band. We have therefore not succeeded in extracting local-orbital shifts for the unoccupied states. The lowest conduction band of the NaCl film is in resonance with the Ge substrate with a width of $\sim$0.5 eV, which also removes the independence of the band energies to the film thickness that we observed for the freestanding films. It is therefore impossible to determine the film's band gap with a sufficient accuracy to detect dielectric response effects.

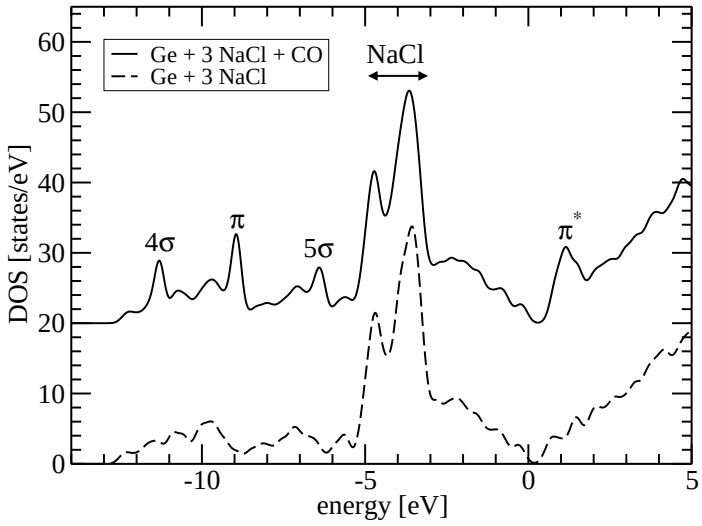

Figure 5.15: LDA DOS for CO adsorbed on a 3 ML NaCl film on Ge. The CO orbitals give rise to sharp peaks.

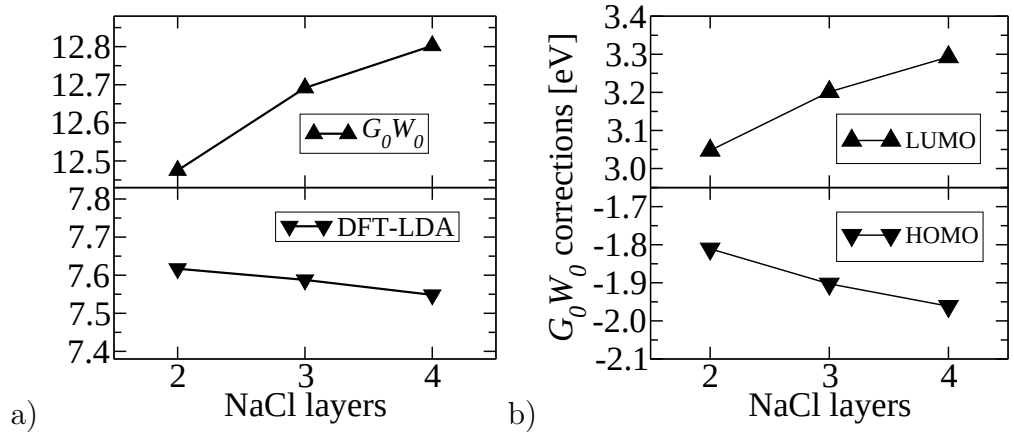

Figure 5.16: a) Molecular gap of CO on NaCl/Ge(001) films at the DFT-LDA and G_0W_0 levels of theory as a function of the film thickness. b) G_0W_0 corrections for the CO highest occupied (HOMO) and lowest unoccupied (LUMO) molecular orbitals.

In order to solve this delocalisation problem for unoccupied states and to demonstrate that not only the film, but also adsorbates on it are affected by the dielectric response of the substrate, we have studied the adsorption of CO on the NaCl films. We note that the CO is the "fruit fly" of surface physics to probe the adsorption and related properties for metal as well as insulator surfaces. We have placed a single CO molecule per p(2×1) unit cell on top of a Na atom with the carbon end pointing towards the surface, which represents the most stable adsorption mode. We have chosen this molecule because it only weakly adsorbs on NaCl and does not introduce a significant perturbation of the NaCl film. In addition, it is a closed shell molecule for which we can perform a G_0W_0 calculation. The CO valence orbitals then serve as a local probe to the image potential. The CO bands are clearly visible in the density of states (cf. Fig. 5.15) and have almost no dispersion in the bandstructure. We have therefore determined the G_0W_0 shifts for the Γ-point only. Already at DFT-LDA, we observe a change of the orbital energies with respect to the Ge vbm when the thickness of the NaCl film is varied. This can mainly be attributed to the change in the work function associated with the thickness change since all CO orbitals are shifted by the same amount.[3] We will therefore concentrate again on the G_0W_0 shifts, shown for films with 2–4 layers in Tab. 5.2. The image-potential effect in the quasiparticle energies amounts to 0.05 eV to 0.15 eV per layer, which is at the limit of the numerical accuracy. We therefore observe a significant numerical noise that prohibits a meaningful quantitative analysis. If a metal were used as a substrate, the image-potential effects would be of course larger. Nevertheless, the qualitative trend is clearly visible. With increasing thickness of the NaCl layer, the occupied CO levels are lowered and the unoccupied levels are raised, thereby increasing the quasiparticle gap (see Fig. 5.16). We thus obtain the same qualitative behaviour for CO on NaCl/Ge as found for benzene on graphite [31]. However, by varying the thickness of the NaCl film the distance of the molecular adsorbate from the Ge substrate can be changed which is impossible for the case of benzene/graphite. Very recently, this effect has been observed in scanning tunneling spectroscopy (STS) for pentacene molecules on NaCl/Cu(111) [6]. For this system, STS allows to determine the molecular HOMO/LUMO gap. For NaCl films of 1, 2, and 3 ML thickness, Repp *et al.* found a pentacene gap of 3.3, 4.1, and 4.4 eV, respectively. This is a considerable reduction compared to the gas phase value of 5.3 eV.

Unfortunately, there is almost no experimental data available for comparison for the NaCl/Ge(001) system, because UPS experiments have focused on the surface properties of thick NaCl films [134]. Possible differences in the UP

[3] With the exception of the 5σ orbital that is involved in the bonding.

		correction [eV]		
	correction method	Ge	NaCl	NaCl - Ge
finite vacuum	dielectric model	+0.08	+0.12	+0.04
finite Ge slab	dielectric model	–0.14	-0.12	+0.02
k-sampling	extrapolation			–0.06
band cutoff	extrapolation	–0.36	–0.43	–0.07
bulk/slab alignment	electrostatic potential	–0.13		–0.13
sum				-0.20

Table 5.3: Corrections for systematic errors in the numerical G_0W_0 calculations to the absolute band positions.

spectra for thin films have not been discussed. The absolute position of the upper NaCl bands with respect to the Ge vbm was reported to be -4.2 eV in Ref. [134], which is in good agreement with our G_0W_0 calculations. For this comparison, we include a correction of -0.2 eV for the systematic modelling errors that we have neglected so far. These are listed in Tab. 5.3 to demonstrate that only few of them significantly affect the relative alignment of the Ge and NaCl states. We note that these effects are largely independent of each other; the corrections should therefore be additive. The most important ones result from low convergence parameters in the numerical G_0W_0 calculations that can be extrapolated very reliably. The reliability was tested for each correction by increasing the corresponding parameter. Using low parameters in the numerical calculation and correcting for them *a posteriori* drastically reduces the computational effort without affecting the accuracy of the final result.

Although the thickness of the NaCl films on the Ge substrate can be well controlled and has been varied for other techniques, e.g. ELS-LEED [133], thickness-dependent photoemission data have not been published for this system. For other thin insulator systems, however, such studies have been performed, e.g. LiCl/Cu(001) [145], MgO/Ag(001) [21], and Al_2O_3/Ru(0001) [140, 146]. In these studies, a variation of the valence band position in UPS [21, 145] or the band gap measured from EELS [140, 146] has been observed upon varying the thickness. It was speculated that image-potential are responsible for this [21, 140, 145]. However, applying our dielectric model to these systems we find only poor agreement for the cases where a quantitative analysis was performed [21, 140]. Compared to the dielectric model, the shifts observed in experiment decay too slowly with increasing thickness and the band width changes comparatively little in contrast to the trend observed in our G_0W_0 calculations. We therefore suggest that other effects, e.g. the

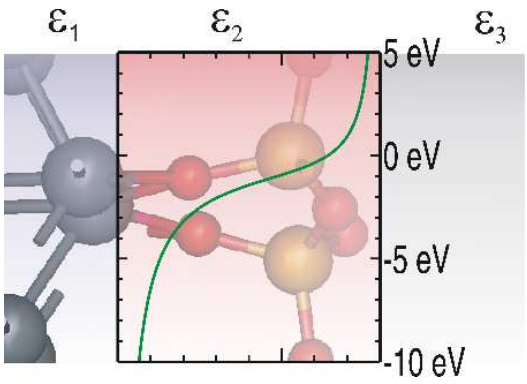

Figure 5.17: The dielectric model for the silica film on Mo(112), rotated by 90°: the Mo (ε_1), SiO_2 (ε_2, and vacuum (ε_3) regions are shaded. The green line shows the image potential.

presence of defects, must be taken into consideration to explain these experiments. On the other hand, NaCl on Ge(001) might be a good model system to experimentally verify the image-potential effects because of the high quality of the films achievable and the possibility to compare to accurate G_0W_0 calculations.

In summary, dielectric response effects are important for a quantitative understanding of the electronic structure of supported insulator films. In contrast to free-standing films, the systematic shifts in the absolute band positions are small because the image effects from the surface and the interface to the substrate oppose each other. Instead, an increase of the band width and a broadening of the peaks in the DOS are observed. The effect of the image potential is most noticeable for (partially) localised states close to the Ge substrate. The Cl atom above the dimer provides such a case, introducing small shoulders at the top of the Cl 3*s* and Cl 3*p* bands that should be detectable in the photoelectron spectra for ultrathin films.

5.3 Image effects in oxide films

We will now return to the oxide films of the previous Chapter and briefly discuss the implications of our findings in this Chapter for these films. Since they are grown on metallic substrates, the dielectric response effects as demonstrated here for the NaCl films on Ge should be even more pronounced due to the larger difference in the respective dielectric constants.

We indeed find experimental evidence that dielectric response effects play an important role in the photoemission spectra of the silica film on Mo(112).

	linkage	inter-row	on-row
ΔV	–0.2 eV	–0.1 eV	±0.0 eV
ΔW	–3.2 eV	–0.7 eV	–0.2 eV
total	+1.4 eV	+0.3 eV	+0.1 eV

Table 5.4: Electrostatic and image potential shifts ΔV and ΔW at the position of the oxygen atoms for SiO_2 on Mo(112). The electrostatic potential at the on-row atom defines the energy zero. The total effect includes the correct prefactor $(-\frac{1}{2})$ for the image potential.

In the crystalline film the O 1*s* core levels of the surface and linkage oxygens as measured by XPS were found to differ by 1.3 eV [13, 105, 108]. This difference was reproduced within DFT [108] by a modified-projector PAW technique that conceptually bases on Slater transition state theory [147].[4] We approach the difference in the core levels in a different way. The ground-state effects are mainly contained in the electrostatic potential at the position of the nucleus, whereas the dielectric response for the core hole is obtained from our dielectric model (cf. Fig. 5.17). Combining the ground-state electrostatic potential shifts with those arising from the core-hole induced polarisation, we are able to reproduce the experimental difference reasonably well (cf. Tab. 5.4). We find that mainly the dielectric response of the Mo(112) substrate is responsible for this difference, while the electrostatic contribution is opposite and small (0.2 eV). We take this as evidence that the dielectric response plays an important role for charged excited states in metal-supported oxide films.

We have also used a model self-energy similar to Eq. 5.4 to compute an image-potential corrected valence DOS for the silica film on Mo(112). Similar to the NaCl film on Ge(001), we find that the height and width of the peak is modified in the upper valence region, but the relative peak positions vary by only 0.1–0.2 eV, because the delocalised states undergo average self-energy shifts. This justifies the use of the uncorrected DOS for discussing the experimental peaks in Sec. 4.3.3. Since the precise peak positions of the model-corrected spectrum sensitively depend on the chosen position of the metal/film interface, we refrain from discussing it in further detail. Strong shifts are found for the localised O 2*s* states that were unfortunately not probed by the UPS experiments since the photon energy of the He^{I} light (21.2 eV) used for these experiments is not sufficient to excite the O 2*s* electrons (binding energy $\approx$ 22 eV). The good agreement achievable for the O

[4] Slater transition state theory takes into account (static) polarisation effects by calculating the self-consistent potential in the presence of an extra charge.

1s core level shifts with our simple electrostatic + image potential approach demonstrates that the dielectric response effects are very important for a quantitative understanding of the photoemission spectra.

We note that image-potential effects for this film were discussed earlier in connection with Si 2p XP spectra. During the growth of the silica films a drift in the Si 2p binding energy was observed in XPS [104, 105]. The shifts were attributed to image effects and explained with a dielectric 3-layer model [105] assuming that the silica film grows layer-wise. However, this is incompatible with the atomic structure of the final film that was not known at that time. Since the final film is only 1 ML thick, an intermediate growth with several different layers below the silicon height in the crystalline film seems unlikely. We therefore believe that the drift in the Si 2p binding energy is not an image-potential effect.

The dielectric response is not only relevant for electron spectroscopy, but generally plays a role for charged states in a supported thin film, at its surface, or for adsorbates. This has recently been demonstrated theoretically for Au atoms on a MgO film on a Mo(100) substrate by Pacchioni *et al.* [121] using DFT. While dielectric response effects for charged excitations are not contained in the DFT band structure because the effective potential is that of the neutral ground-state, the total energy reflects them when the extra charge is explicitly considered or if the ground-state involves a charge transfer.[5] The ground-state surface properties of the MgO film do not differ strongly between a free-standing and a supported film and are converged at $\sim$3 ML in both cases. However, the adsorption of gold atoms differs drastically between free-standing and supported films. In this particular case, the presence of the metal substrate alters the charge state for adsorbed Au atoms, which become Au^-. Pacchioni *et al.* have found a significant thickness dependence of the adsorption energy which they attributed to the difference in the image potential [121].[6] While the metal-induced change of the adsorbate's charge is probably an extreme case for the influence of the metal substrate, the dielectric response of the substrate certainly affects the stability of charged adsorbates [121] or charged defects at the surface [91]. This has dramatic consequences for the use of supported oxide films as model supports for heterogeneous catalysts. The image potential induced

[5]This is also the reason why Slater transition state theory accounts well for the polarisation effects. However, the factor 1/2 arising from the adiabatic switching on of the induced potential is put in by hand.

[6]However, the magnitude of the effect in the calculation may have been enhanced by the use of a finite metal slab. Since the electron for Au^- is taken from the metal, the metal slab will acquire a finite excess charge density which adds an electrostatic contribution to the interaction energy.

by the substrate directly modifies the energetics of all charged states at the surface of the oxide film and of adsorbates on it. Moreover, this influence is invisible in the absence of charged states, i.e. neutral spectroscopies like optical absorption or EELS will not show this effect.

Likewise, charge carrier processes in oxide films used in electronic devices may be influenced by image potential effects. Since the films have two identical (or at least dielectrically similar) surfaces, the situation is comparable to free-standing films, but with opposite sign. In electronic device applications, the oxide films are embedded in a material with a higher dielectric constant. The image potential therefore reduces the band gap, thereby lowering the barriers for electron tunnelling. From the NaCl films, which have a similar electronic dielectric constant as the oxides, we estimate that such effects become relevant (i.e. exceed 0.1 eV) at thicknesses below $\sim$10 Å, depending on the dielectric constant of the oxide and of the surrounding semiconductor or metal. For a specific combination of dielectric constants, simple dielectric slab models can provide an upper estimate of the effect.

5.4 Summary

In this Chapter we have presented G_0W_0 quasiparticle calculation for free-standing and supported thin insulator films, using NaCl as a prototypical example. We have shown that the surface polarisation in free-standing films and the dielectric response of a substrate introduce important changes beyond the shifts in the bulk materials. Thereby, free-standing and supported films behave quite unlike: In free-standing films the quasiparticle gap increases. When, on the other hand, the film is supported on a substrate with a higher dielectric constant the self-energy becomes position-dependent, leading to non-uniform G_0W_0 corrections within the valence and conduction bands of the LDA. These effects can be qualitatively understood with simple dielectric models, but a full G_0W_0 calculation for the supported system is necessary if quantitative results are required. We have then presented evidence that image effects are also visible in the metal-supported oxide films. Finally we have discussed other properties besides the quasiparticle spectrum that may be affected by the dielectric response effects.